



Recommendations for generating dispersion images of optimal resolution from active MASW survey

Jumrik Taipodia¹ · Dipjyoti Baglari² · Arindam Dey³ 

Received: 26 October 2017 / Accepted: 13 December 2017 / Published online: 4 January 2018
© Springer International Publishing AG, part of Springer Nature 2018

Abstract

Multichannel Analysis of Surface Waves (MASW) is proving to be the most recent and popular non-invasive method which can characterize the subsurface in quick and better ways. This article reports a detailed study of active MASW survey conducted in a soil site characterized by the presence of heterogeneous soil stratification with crushed debris. In this regard, the effect of receiver layout and key data acquisition parameters (offset distance, far-field and near-field phenomena, receiver spacing, total receiver spread length and numbers of deployed receivers) on the resolution of the obtained dispersion image is elucidated. The influence of the signal pre-processing parameters such as sampling frequency, sampling length, filtering and muting, is also highlighted. The effect of source characteristics on the quality of the recorded wavefield has been elaborated, and in this context, the enhancement of the resolution of dispersion image by stacking has also been discussed. Based on the outcomes, it is recommended that the sampling frequency and sampling time should be optimal so that complete propagation of wave phases through the geophone array is achieved, while at the same time, the time-stamp suffers minimum noise adulteration. Combined application of band-pass filtering and optimal temporal muting is required to obtain best resolution dispersion images. For sites having predominantly softer soils at the shallower depths ($V_{s,30} < 100$ m/s), an optimal offset of 4–6 m with an inter-receiver spacing of 1 m produces the best resolution dispersion images. The resolution of the dispersion image at the lower frequencies can be increased either by using a heavier source, or adopting multiple stacking of dispersion images generated from low energy impacts.

Keywords MASW · Dispersion image · Resolution · Sampling frequency · Stack · Filtering

Introduction

Multichannel Analysis of Surface Waves (MASW) is a non-destructive seismic exploration method for evaluating stiffness of the subsurface in 1D, 2D and 3D formats. It is a surface-wave method [1] in which the waves are generated

by various impact sources such as sledgehammer, automatic generator, electro-mechanical shakers or bulldozers. The generated waves are recorded by an array of geophones, which are analyzed to obtain a shear wave velocity profile of the substratum. In comparison to the conventional borehole survey methods, MASW proves to be less expensive, less time consuming, and can overcome the inherent limitation of conventional borehole surveys in establishing the heterogeneous stratification of the subsurface. The MASW approach has been used by many researchers at different locations round the world, aiding in the identification of both shallow and deeper subsurface stratification [2–9]. The three basic steps of the MASW approach consist of data acquisition, dispersion analysis and inversion analysis. The inference from the MASW survey largely depends on the clarity and resolution of the dispersion images developed from the wavefields collected during the field experimentation. Despite being quite popular currently, there is a dearth of accepted guidelines which can be followed stage-wise to

✉ Arindam Dey
arindamdeyitg16@gmail.com

Jumrik Taipodia
jtaipodia@gmail.com

Dipjyoti Baglari
dipjyoti.baglari@gmail.com

¹ Department of Civil Engineering, NIT Arunachal Pradesh, Papum Pare, India
² Department of Civil Engineering, Jorhat Institute of Science and Technology, Jorhat, India
³ Department of Civil Engineering, Indian Institute of Technology Guwahati, Guwahati, Assam 781039, India

obtain good resolution dispersion images. It is well understood that the resolution of the experimental dispersion image will be largely affected by various data acquisition, processing and pre-processing parameters (e.g. sampling frequency, length of samples, muting, filtering, stacking, offset distance, receiver spacing, source used, total number of channels, source energy). Hence, it is imperative to rigorously understand their effects on the dispersion image and its resolution. In this regard, the article reports about an exhaustive active MASW investigation conducted at a specific location at IIT Guwahati. The raw signals, generated from the impacts at the ground surface by means of a sledgehammer or Propelled Energy Generator (PEG), were collected using a linear array of geophones. The raw wavefield records were pre-processed through filtering and muting to obtain signals capable of generating high resolution dispersion image. The extracted experimental dispersion image was subjected to inversion analysis to obtain the shear wave velocity profile of the subsurface. Based on the distinctness and resolution of the generated dispersion image and the obtained shear wave velocity profile, certain recommendations related to the choice of the contributory parameters are framed.

Active MASW investigation

The present study is based on active MASW tests carried out at Core-4 of the Academic Complex at IIT Guwahati, India (Fig. 1a). The site primarily comprises heterogeneous layers of soil and crushed debris. Cross-hole tests conducted at the location revealed that the shear wave velocities within

a depth of 7 m, at the site, are below 100 m/s (Fig. 1b). Figure 2 shows the schematic diagram of the Active MASW survey conducted in the field. In general, the seismic waves generated through an impulse hammer strike propagates through soil substrata and are eventually recorded by a set of geophone receivers placed in a linear array. The receivers are connected to a Data Acquisition System (DAQ) comprising a seismograph. In the present study, 12 or 24 numbers of 4.5 Hz geophones, placed in a linear array, have been used to record the seismic signals generated by a 10 kg sledgehammer and a 40 kg PEG. The equipment used in the present study is shown in Fig. 3. Experiments with various geophone configurations were conducted in order to investigate the effects of offset distance, far-field and near-field phenomena, receiver spacing, total receiver spread length,

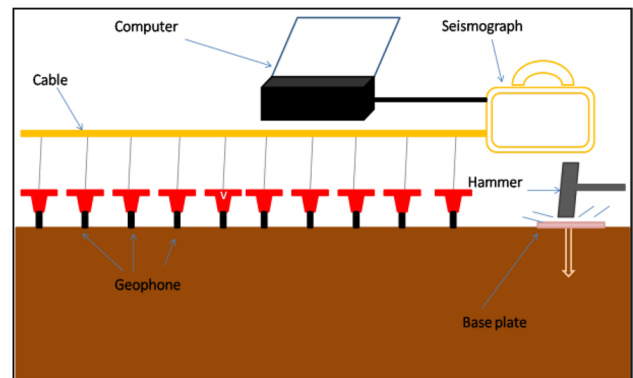
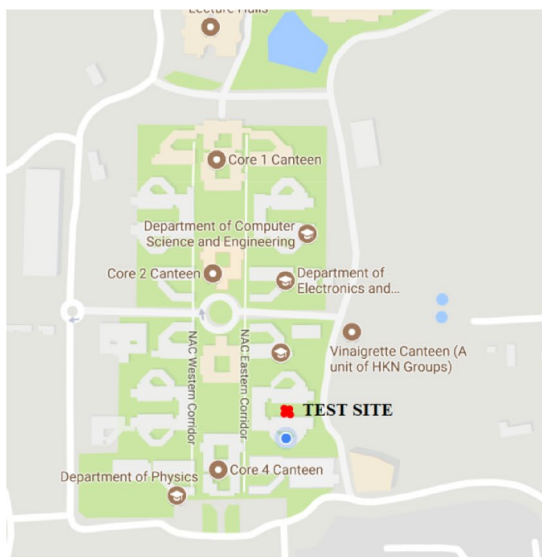
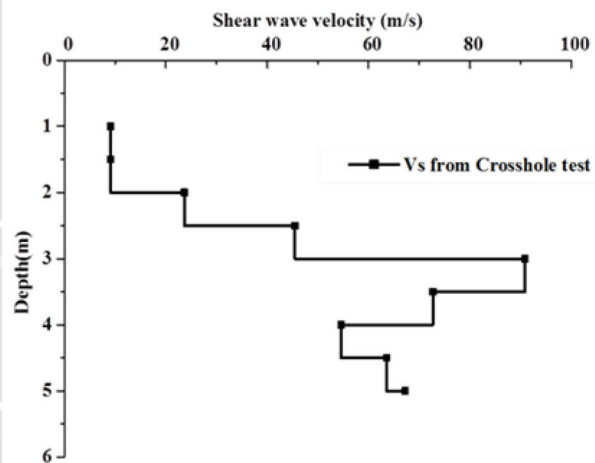


Fig. 2 Schematic representation of active MASW survey



(a)



(b)

Fig. 1 a Chosen site for active MASW survey (Google images), b Shear wave velocity profile at the site as obtained from the cross-hole seismic survey

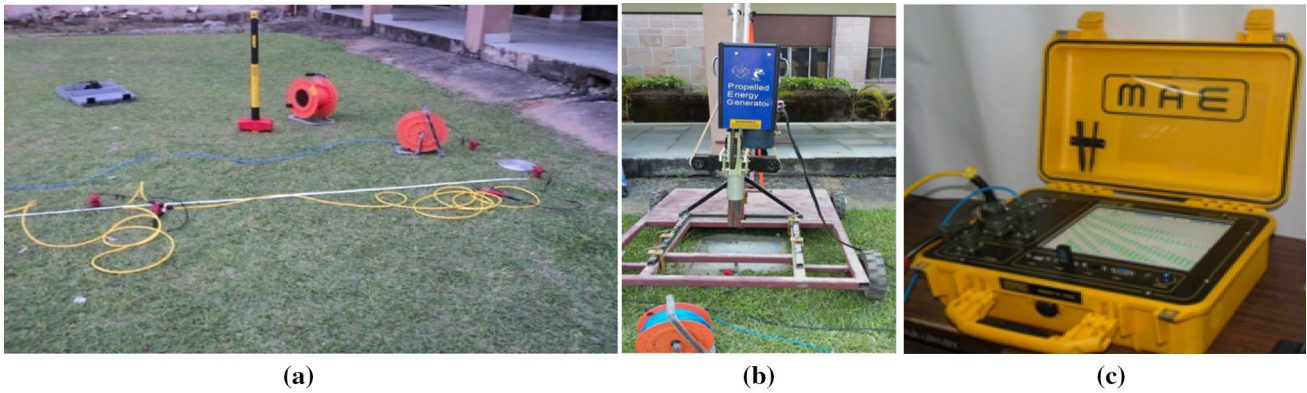


Fig. 3 Accessories of active MASW survey: **a** 10 kg sledgehammer, 4.5 Hz geophones, cable connections and striker plate, **b** 40 kg PEG, **c** MAE seismograph as DAQ

numbers of deployed receivers, and type of source on the generation of a good resolution dispersion image.

Dispersion analysis and resolution of dispersion image

Dispersion of seismic waves is the phenomenon related to a cylindrical or hemispherical wave front travelling through the soil medium, where each of the propagating wave frequencies can possess multiple phase velocities, and vice versa. When more than one phase velocities exist for a given frequency, the phenomenon corresponds to multimodal dispersion. The dispersion curve having the slowest phase velocities corresponds to the fundamental

mode (M0), while the next faster one corresponds to the first higher mode (M1), and so on. In the multichannel approach, dispersion analysis results in a tri-dimensional frequency–phase velocity ($f-C$) image space from which the dispersion trends are identified from the pattern of energy accumulation (Fig. 4). The dispersion image is generally obtained by applying Fast Fourier Transform (FFT), or similar techniques, on the recorded wavefields processed through frequency filtering and muting [1]. The power spectral amplitude in the frequency domain indicates the distribution of the recorded energy over a frequency band. From any dispersion image, the fundamental and/or higher modes of dispersion curves are extracted by following the image trends of localized maximum energy accumulation.

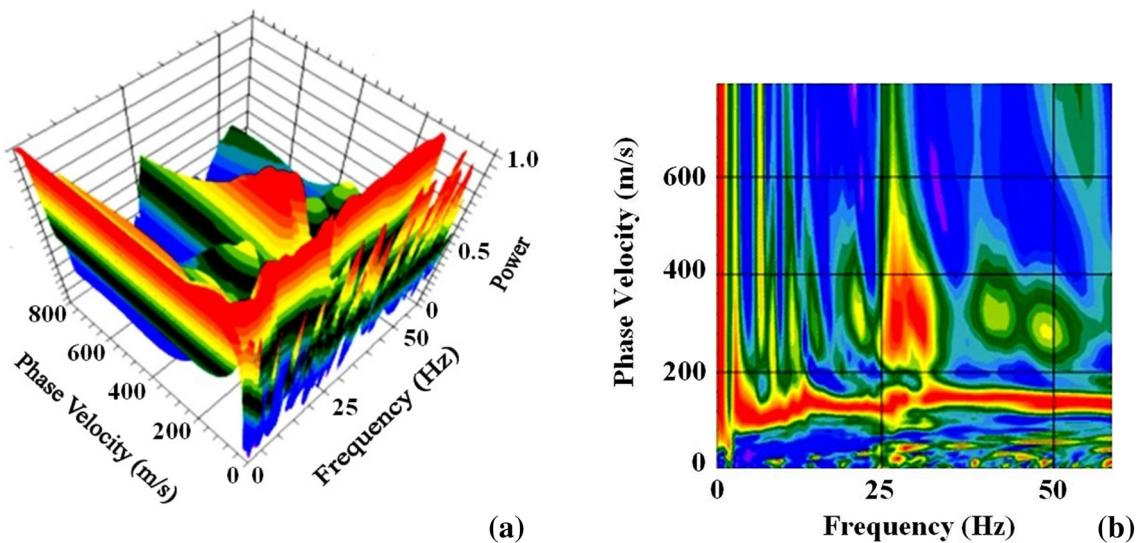


Fig. 4 Dispersion image as the inter-relationship between frequency, phase velocity and energy concentrations **a** triaxial representation, **b** biaxial representation

Resolution of an image is defined by the number of pixels contained in a unit area, and is commonly expressed in various units such as lines per mm (l pm), lines per inch (l pi), and, more commonly, dots per inch (dpi). Park et al. [1] defined the resolution of a dispersion image as the resolvable capabilities along both the velocity and frequency axes. The accuracy and resolution of surface wave dispersion analysis depends on the data acquisition parameters adopted for the field investigation [10, 11]. A detailed review on the resolution of dispersion image obtained from active MASW survey has been elaborated by Taipodia et al. [12]. From various literatures, it can be concluded that a dispersion image possesses good resolution if it exhibits a distinguishable trend of dispersion curve, with clearly identifiable fundamental and/or higher modes within a wide frequency band. The image should exhibit narrow and concentrated energy signature so that, based on the local maximum energy accumulations, the dispersion curves can be easily extracted to be subsequently used for inversion analysis. Based on exhaustive active MASW surveys, this article attempts to frame certain guidelines to obtain the dispersion images with the best possible resolution.

Results and discussions

Effect of sampling frequency and sampling time

Sampling frequency or the sampling rate, f_s , is the average number of samples obtained in one second (samples per second, sps), thus $f_s = 1/T$, where, T is the sampling interval (seconds). In order to avoid aliasing, Sauvin et al. [13] suggested to use a sampling interval of 1-ms with a 1 s recording time. If the recorded traces are truncated by a very short time window, a portion of the low velocity energy is lost leading to the overestimation of the propagation velocities. On the other hand, if the sampling frequency is excessively

high, unwanted noise would alter and adulterate the signal generated from the actual impulse. In active survey, the waves produced are mostly high frequency waves possessing smaller penetrating depths within the subsurface. For these waves, moderately high sampling frequency is suggested to obtain the best possible dispersion image. Time of acquisition (t), or the total sampling time, is defined as the total number of recorded samples (n) per unit sampling frequency (i.e. $t = n/f_s$). The acquisition time increases with the increase in the number of recorded samples. However, a too high sampling time will result in recording significant noise leading to the contamination of the useful signal. Hence, it is imperative to use an optimal sampling time and the required sampling frequency. The choice of sampling frequencies and time of sampling by different researchers has been random and as per the suitability, without proper scientific reasoning behind the choices [14–16].

For the present study, varying length of the samples have been used (i.e. 5120, 10,240, 20,480), along with different sampling frequencies (15,000, 7500, 3750, 2000, 1000, 500, 100 and 50 Hz). Corresponding to a fixed sample length of 5120 samples, Fig. 5a–d illustrates the MASW raw records collected for few chosen sampling frequencies. It is clear that time of sampling is dependent upon the choice of sampling frequency. Figure 5a shows that sampling frequency 15,000 Hz resulted in a record time of 341 ms, within which all the predominant wave phases have been completely recorded by the geophone array. As the sampling frequency decreased, the time of acquisition increased, resulting in progressively more and more noise contamination for lower sampling frequencies (Fig. 5b–d). In each of the later cases, although the propagation of the predominant phases has been complete, increased sampling time attracted higher levels of noise adulteration, especially in the far-off geophones. Hence, it is necessary to choose an optimum sampling time so that the necessary propagating wave phases get completed without significant noise adulteration in the

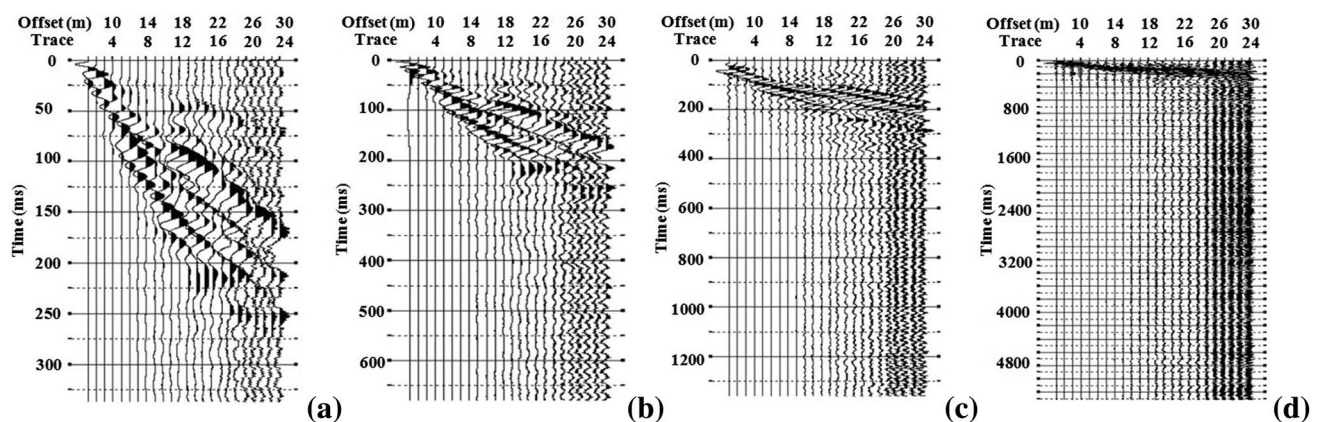


Fig. 5 Effect of sampling frequency on time records obtained for 5120 samples **a** 15,000 Hz, **b** 7500 Hz, **c** 3750 Hz, **d** 1000 Hz

recorded wavefield. Corresponding to the collected time-stamps exhibited in Fig. 5, the dispersion images for different sampling frequencies (15,000, 7500, 3750 and 1000 Hz) are shown in Fig. 6a–d. It can be seen that the distinctness in the dispersion image gradually reduces with the decrease in the sampling frequency. The dispersion image for the sampling frequencies less than 1000 Hz was beyond consideration due to excessive noise adulteration in the time stamps.

Correspondingly to a sampling frequency of 15,000 Hz, Fig. 7 exhibits the effect of numbers of recorded samples on the procured wavefield. It is observed from Fig. 7a that a sample length of 5120 (Sampling time = 341 ms) is just sufficient to capture the complete phase propagation through the geophone array. Higher number of samples (10,240 and 20,480), induces higher sampling time (682 and 1365 ms),

and allows the propagation phases to be complete as well. However, with the higher sampling length, more noise adulteration can be observed at the far-off geophones. Figure 8 exhibits that a comparatively better resolution dispersion image is obtained corresponding to the record length of 5120 samples. For the other cases, the dispersion images show aliasing effects in the lower frequencies due to noise adulteration in the far-off geophones. Similar observations are reflected in the wavefield collected using sampling frequency of 7500 Hz, as shown in Fig. 9. It can be observed that even for this case, 5120 samples are sufficient to capture the completion of the wave propagation through the array, further increase in number of samples leads to higher degree of noise adulteration. However, a comparison of Figs. 7a and 9a evidently suggests that the level of noise adulteration in

Fig. 6 Dispersion images corresponding to 5120 samples having different sampling frequencies **a** 15,000 Hz, **b** 7500 Hz, **c** 3750 Hz, **d** 1000 Hz

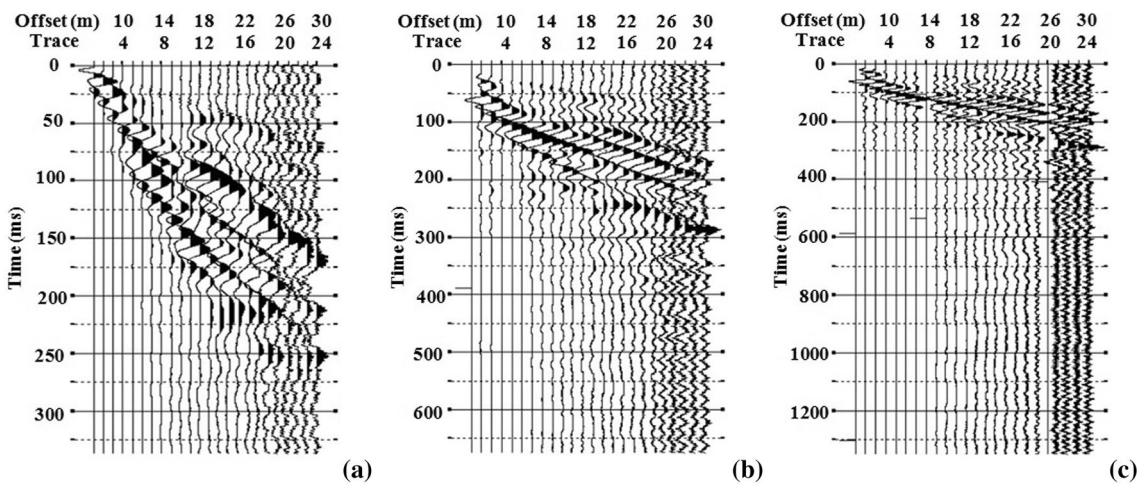
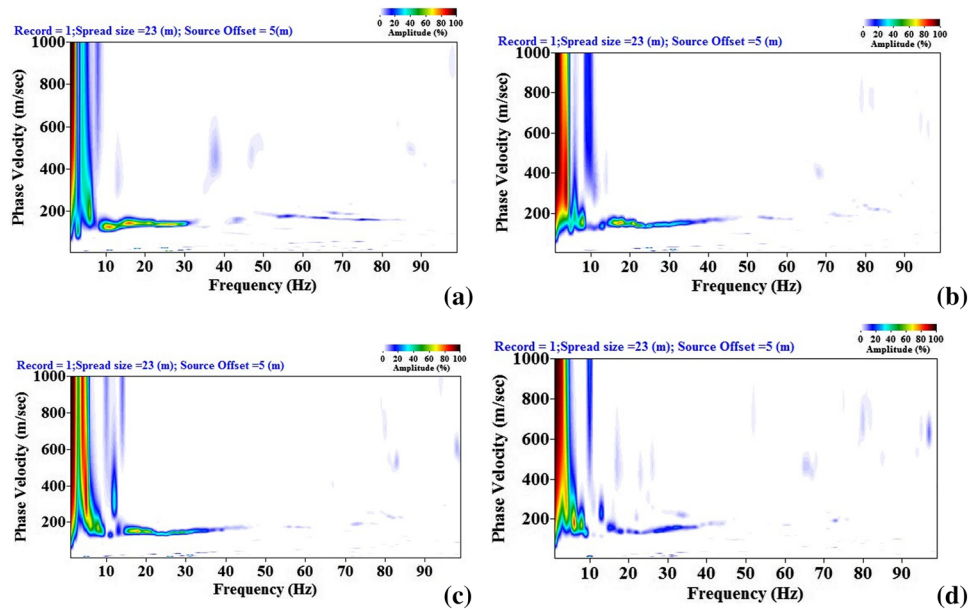


Fig. 7 Collected time records having sampling frequency 15,000 Hz with varying number of samples **a** 5120, **b** 10,240, **c** 20,480

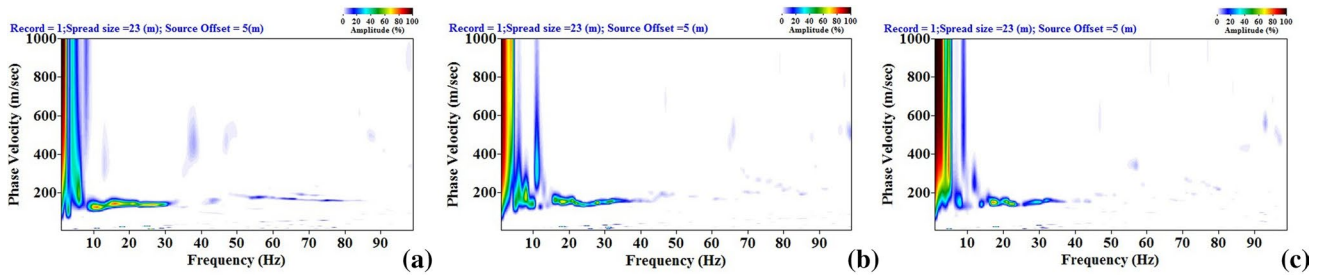


Fig. 8 Dispersion images developed from the collected time records having sampling frequency 15,000 Hz with varying number of samples **a** 5120, **b** 10,240, **c** 20,480

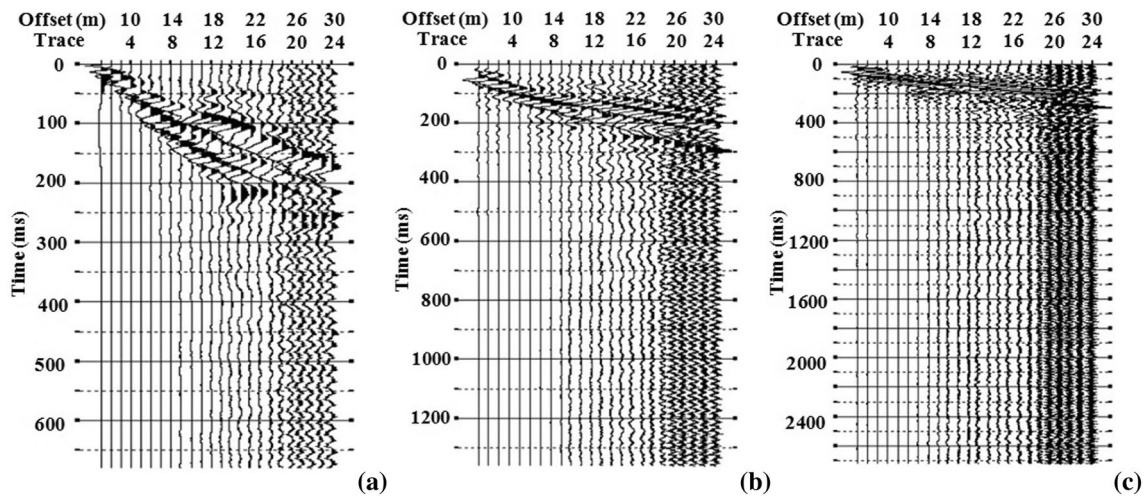


Fig. 9 Collected time records having sampling frequency 7500 Hz with varying number of samples **a** 5120, **b** 10,240, **c** 20,480

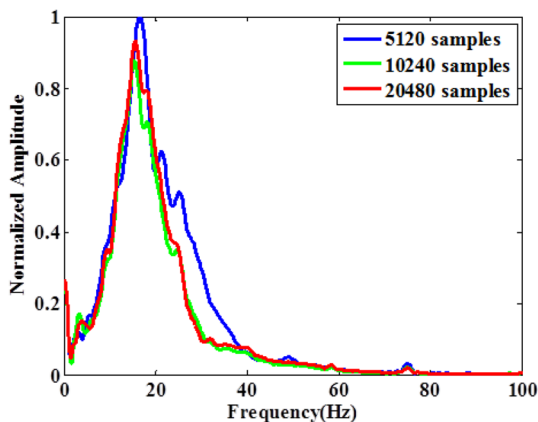


Fig. 10 Normalized amplitude spectra obtained for different sample lengths with sampling frequency 15,000 Hz

the far-off geophones is lesser for the sampling frequency of 15,000 Hz.

As observed from the amplitude spectra obtained for the sites (Fig. 10), it can be understood that the length of the

samples does not have a significant effect on the quality of the collected record, provided the phase of wave propagation is completely captured. It can be seen that for a particular site, the normalized amplitudes are tolerably same for different length of the samples. Based on the above study, an optimal sample length of 5120 samples for sampling frequency 15,000 Hz was found suitable and chosen for the chosen site for further processing. Figure 10 also indicates the range of frequencies over which the energy of wave propagation is concentrated. The range is between 18 and 20 Hz.

Based on the above observations, it can be stated that for any particular site, the complete phase of wave propagation through the geophone array can be tracked by various combinations of sampling frequency and sampling length. Among the possible combinations, choosing the one with higher sampling frequency provides a higher resolution dispersion image. The conventional notion that the resolution of the dispersion image increases with the increase in sampling frequency is not always necessarily true, and also depends on the sampling time. It is important that only an optimal time is chosen so that the collected records are complete

and free from the adulterating noise to the highest possible extent. Before carrying out any rigorous experimentation at a particular site, it is recommended to check whether the chosen sampling frequency is appropriate by reading the recorded phase propagation pattern.

Effect of frequency filtering and muting

Frequency filtering is commonly applied to the raw wavefields to enhance the resolution of dispersion image by suppressing the adulterating noise, mostly associated with higher frequencies [17, 18]. As per the conventional filtering theory, four variants of filtering commonly applied are the low-cut (only high frequencies are allowed to pass), high-cut (only low frequencies are allowed to pass), band-cut (a band of frequencies is restricted from passing) and band-pass (only a specific frequency band is allowed to pass). In the present study, the commercial software SURFSEIS, in which all the above-stated filtering techniques are inbuilt, has been used to check their efficacy in obtaining a good resolution dispersion image. Muting is a pre-processing task adopted for optimal removal of body wave and other low amplitude noises intruded in the raw wavefield. It is performed by selecting two limiting scanning phase-velocities on the wavefield, meant for top-muting and bottom-muting,

and thus resulting in an exclusive noise-cone removal from the collected records [19].

Filtering is carried out based on the response of the amplitude spectrum to the applied filter as shown in Fig. 10. For the chosen site, the amplitude spectra indicates that the effective frequency content ranges between 2 and 80 Hz, and the same has been adopted in the present study for various filtering approaches are listed in Table 1.

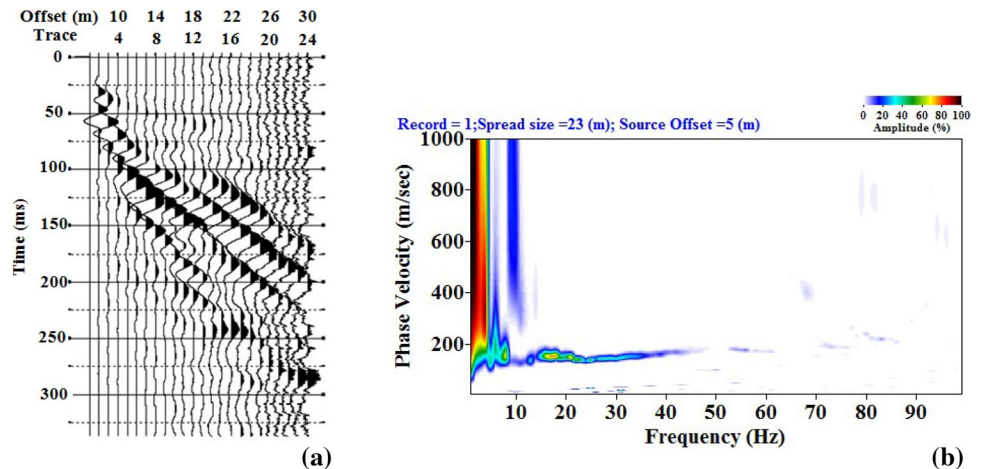
Figure 11 shows a raw wavefield and its corresponding dispersion image, obtained with a field receiver configuration of 4 m offset, 1 m receiver spacing, and 24 numbers of geophones in a linear array having a total spread length of 23 m. Figure 11a shows that the unfiltered raw data is obscure in the last few traces indicating noise contamination. The corresponding dispersion image (Fig. 11b) is of low resolution, thus making it ambiguous to extract the dispersion curve. Moreover, a significant energy is solely accumulated in lower frequency range (< 10 Hz) indicate noise contamination originating from the low frequency waves. These raw wavefield is used as a base figure for further elucidating the effects of filtering and muting.

Figures 12 and 13 highlight the effect of various filters on the raw wavefield and their corresponding dispersion images. It is observed that the application of band-stop filter (Fig. 12b) and low-cut filter (Fig. 12d) alters the characteristics of the raw wavefield by removing a significant amount of energy content. The corresponding dispersion images (Fig. 13b, d) exhibit a high degree of obscurity and do not show any formation of the M0 dispersion curve, and hence, are beyond any purposeful utility. Based on this observation, it is recommended to avoid the use of band-stop and low-cut filters to analyze the signals obtained from active MASW survey. This observation is similar to the findings of Park et al. [20]. Both band-pass (Fig. 12a) and high-cut (Fig. 12c) filters are effective in removing the unwanted noise to a reasonable extent. However, the dispersion image obtained from band-pass filtering (Fig. 13a) exhibits a long and

Table 1 Frequency ranges for various filtering applications adopted in the present study

Filter type	Frequency range			
	f_1 (Hz)	f_2 (Hz)	f_3 (Hz)	f_4 (Hz)
Band-pass	2	10	70	80
Band-cut	2	10	70	80
High-cut	–	–	70	80
Low-cut	2	10	–	–

Fig. 11 a Unfiltered wavefield, b corresponding dispersion image



distinct energy trend in the fundamental mode in comparison to the same obtained from the high-cut filter (Fig. 13c). In such a case, the extraction of the M0 dispersion curve becomes easier, since it is possible to locate the peak energy points at various frequencies with greater reliability. Based on the above observations, the band-pass filter proves to be efficient in generating good resolution dispersion images.

For the present study, band-pass filter of 2–10–70–80 Hz specifications resulted in the best dispersion images from the tests conducted at the site.

The effect of extent of muting conducted on the unfiltered record (Fig. 11a) is exhibited in Fig. 14. Excessive muting may result in significant characteristic loss, and hence, muting should be controlled so that an optimum energy content

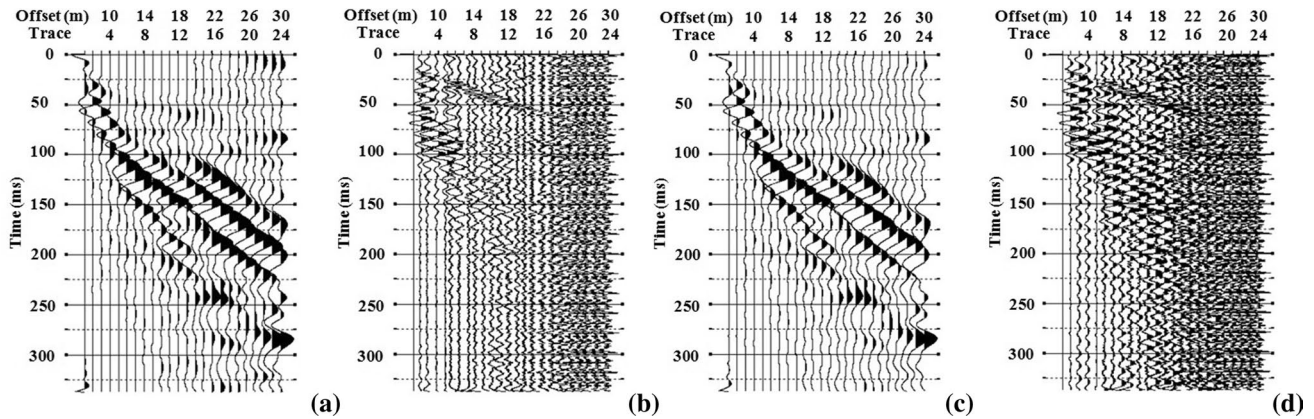


Fig. 12 Modified MASW records obtained from different filtering techniques **a** band-pass, **b** band-stop, **c** high-cut and **d** low-cut

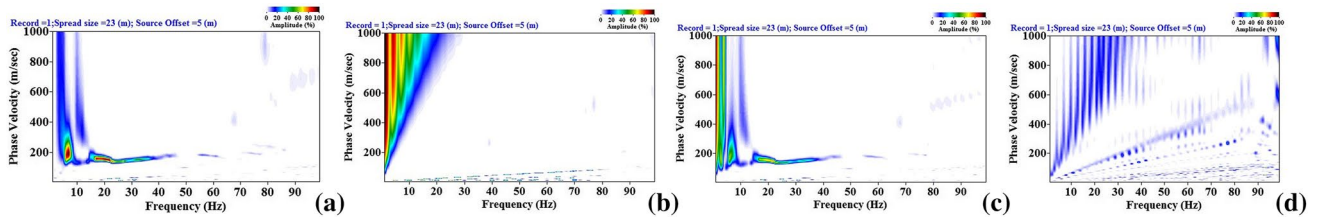


Fig. 13 Dispersion images obtained from different filtering techniques **a** band-pass, **b** band-stop, **c** high-cut and **d** low-cut

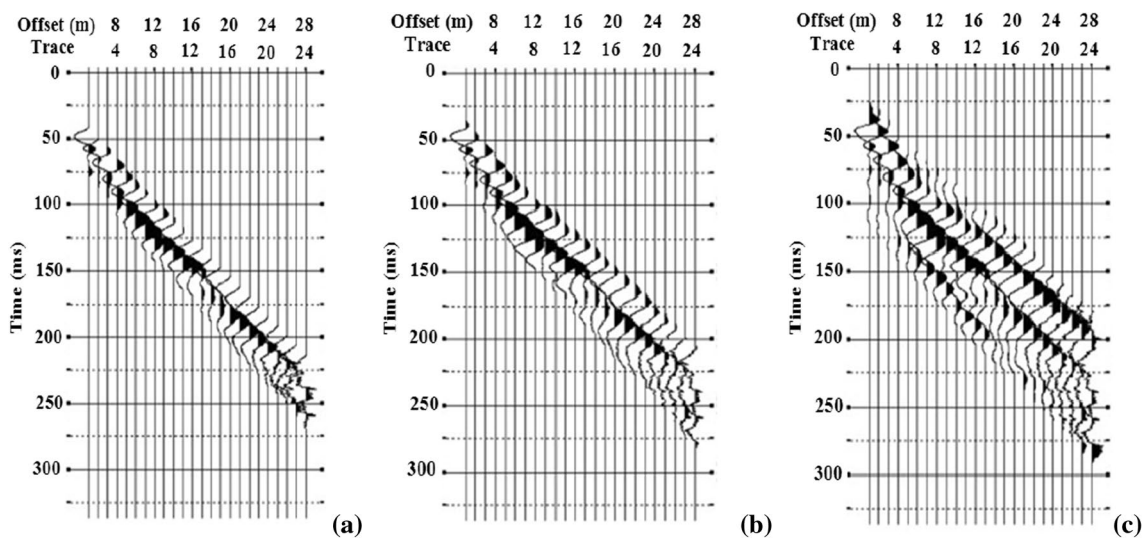


Fig. 14 Effect of different extents of muting on the wavefield pattern **a** excessive muting, **b** moderate muting, **c** minimal muting

of the signal is maintained while removing the adulterating noises. Figure 14a shows the outcome of excessive muting which has resulted in a modified wavefield with a single wavelength of the original record; similarly, Fig. 14d shows the result when minimal muting is carried out to remove the noise adulterations. The corresponding dispersion images are presented in Fig. 15. It can be observed that due to excessive muting (Fig. 14a), significant energy is lost, and hence, the corresponding dispersion image (Fig. 15a) fails to provide the M0 dispersion curve. As the extent of muting decreases (Fig. 14b–c), the corresponding dispersion images gain more clarity with distinct M0 regions (Fig. 15b–c). However, at the same time, the energy concentration at the lower frequencies also increases, thus exhibiting an enhanced aliasing effect. Thus, it can be stated that muting alone on unfiltered signals cannot generate a dispersion image with sufficient information and good resolution. Hence, muting is recommended on filtered wavefields for proper dispersion images with good resolution.

Based on the above discussions, different combinations of muting and filtering have been applied on the raw wavefield. Figure 16a shows data raw wavefield record obtained, while Fig. 16c–d depicts the modified wavefield records after processing through only muting (Fig. 16c), only filtering

(Fig. 16d), and both filtering and muting (Fig. 16d). It can be observed that application of both filtering and muting techniques produces the best quality wavefield records.

Figure 17 exhibits the dispersion images obtained from varying extents of muting conducted on band-pass filtered wavefield. Compared to the dispersion images obtained from unfiltered wavefields (Fig. 11b), it can be clearly observed that the same obtained from the muted and filtered wavefields exhibit better resolution, since substantial noise is eliminated in the process. As observed earlier, excessive muting results in significant information loss and renders a comparatively poor resolution dispersion image. Based on the obtained dispersion images, the optimal extent of the muting of the filtered wavefield can be suitably decided.

Effect of receiver layout and configuration

Effect of offset distance

Offset distance is defined as the linear distance between the source and the first receiver geophone. Two prevalent phenomena due to varying offset distance are the near-field effect and the far-field effect [21, 22]. The near-field effect represents the unpredictable non-planar propagation of

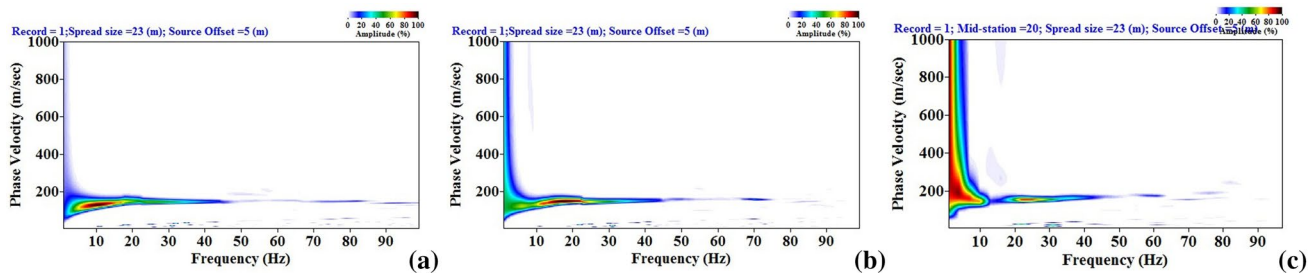


Fig. 15 Effect of different extents of muting on the generated dispersion images **a** excessive muting, **b** moderate muting **c** minimal muting

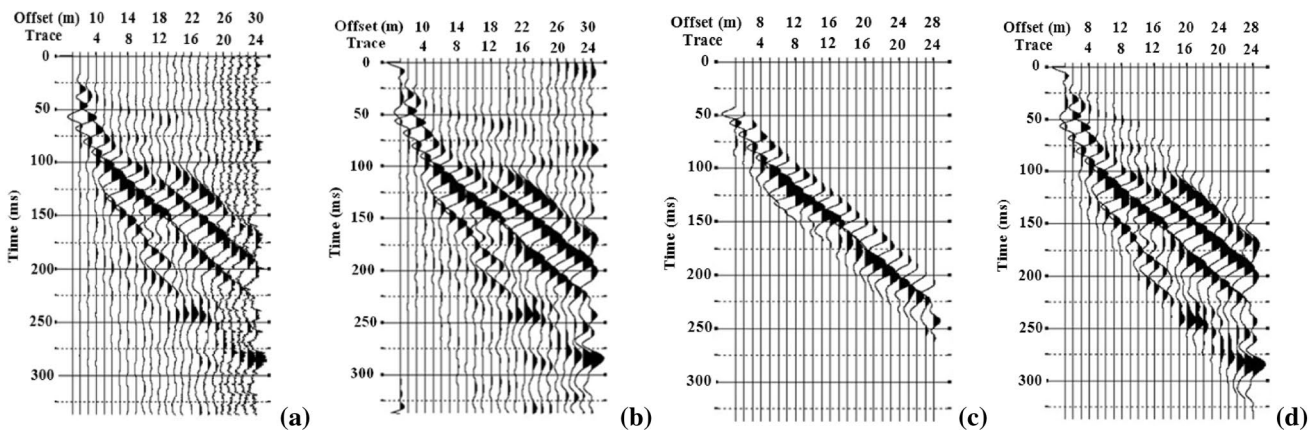


Fig. 16 Typical wavefield record **a** raw, **b** only filtered **c** only muted, **d** combined filtered and muted

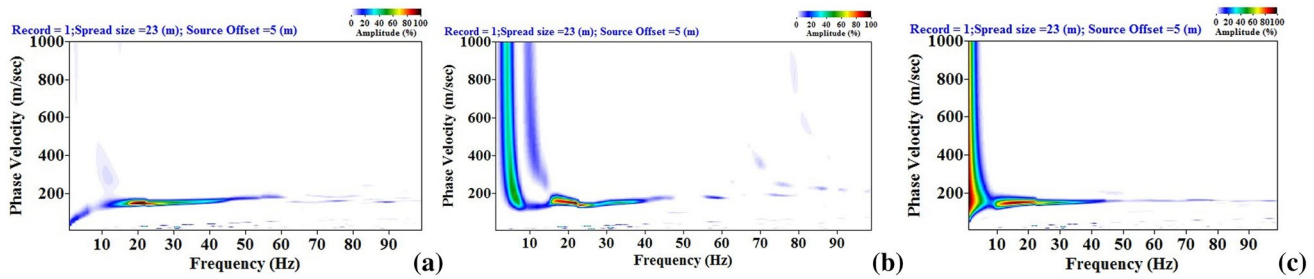


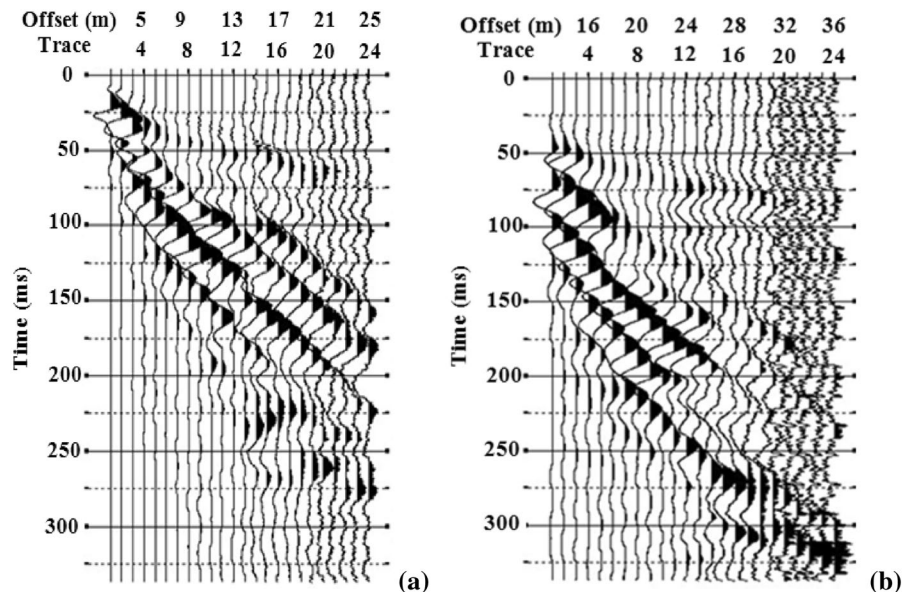
Fig. 17 Effect of extent of muting on dispersion image obtained from band-pass filtered wavefield **a** excessive muting, **b** moderate muting, **c** minimal muting

surface waves near the source point caused by generation of excess stresses, which are eventually responsible for underestimated phase velocities of relatively long wavelengths. Surface waves become planar after travelling a certain distance from the source [21, 23]. The near-field effects are associated with the minimum distance required for planar surface waves to develop, and is governed by the interference of multiple reflections and mode conversions of body waves at the free surface. Since, the surface wave method requires the analysis of horizontally travelling plane waves, it is important to avoid recording of any non-planar components. Qualitatively, a longer wavelength traverses a larger distance to become planar. Far field effects indicate that signal corresponding to the surface waves either become relatively weak at larger distances (due to attenuation and geometrical spreading), or are contaminated by prevalent undesirable noise wave field (e.g. traffic noise, random ambient noise, scattered surface waves and body waves) [22]. The contamination can also be caused by higher modes of surface waves that may prevail at far offsets because of their

relatively smaller attenuation. If these contaminated wave fields are included in the analysis for dispersion imaging, they tend to cause destructive interference on the computation of the phase velocity–frequency relationship, and hinder from obtaining large amplitude in the image space. Preliminary guidelines for the near-offset and far-offset effects are proposed by few researchers [10, 11, 20, 24].

In the present study, in order to check the far-field and near-field effect on the resolution of dispersion image, experiments were carried out with different offsets (varying in the range of 0–15 m), sampling frequencies (7500–15,000 Hz), and receiver spacing (1–3 m), accompanied by varying number of receivers (12 and 24). All the collected field records were treated with Band-pass filtering and temporal muting. Three vertical stacking of the dispersion image have been used to increase the resolution of the obtained dispersion images. Figure 18 shows the effect of offset distance, where it can be clearly observed that a larger offset distance result in a higher time-lag for the receivers to commence recording the signals. Moreover, the far-off geophones are found to

Fig. 18 Typical wavefield obtained for different offsets **a** 1 m, **b** 12 m



record higher levels of noise from the surrounding medium when a large offset is used.

Figure 19 shows the effect of the near-field and far-field offsets on the obtained resolution of dispersion image. Figure 20 shows the inverted shear wave velocity profiles obtained from the analysis of the signals collected using

various offset distances. It can be observed that due to significant interference from body waves, the M0 dispersion images obtained using near offsets (0–3 m, Fig. 19a–d) does not exhibit a distinct energy trend; rather, displays a discontinuous trend with an unnaturally high accumulation of energy at low frequencies. Dispersion curves, extracted by

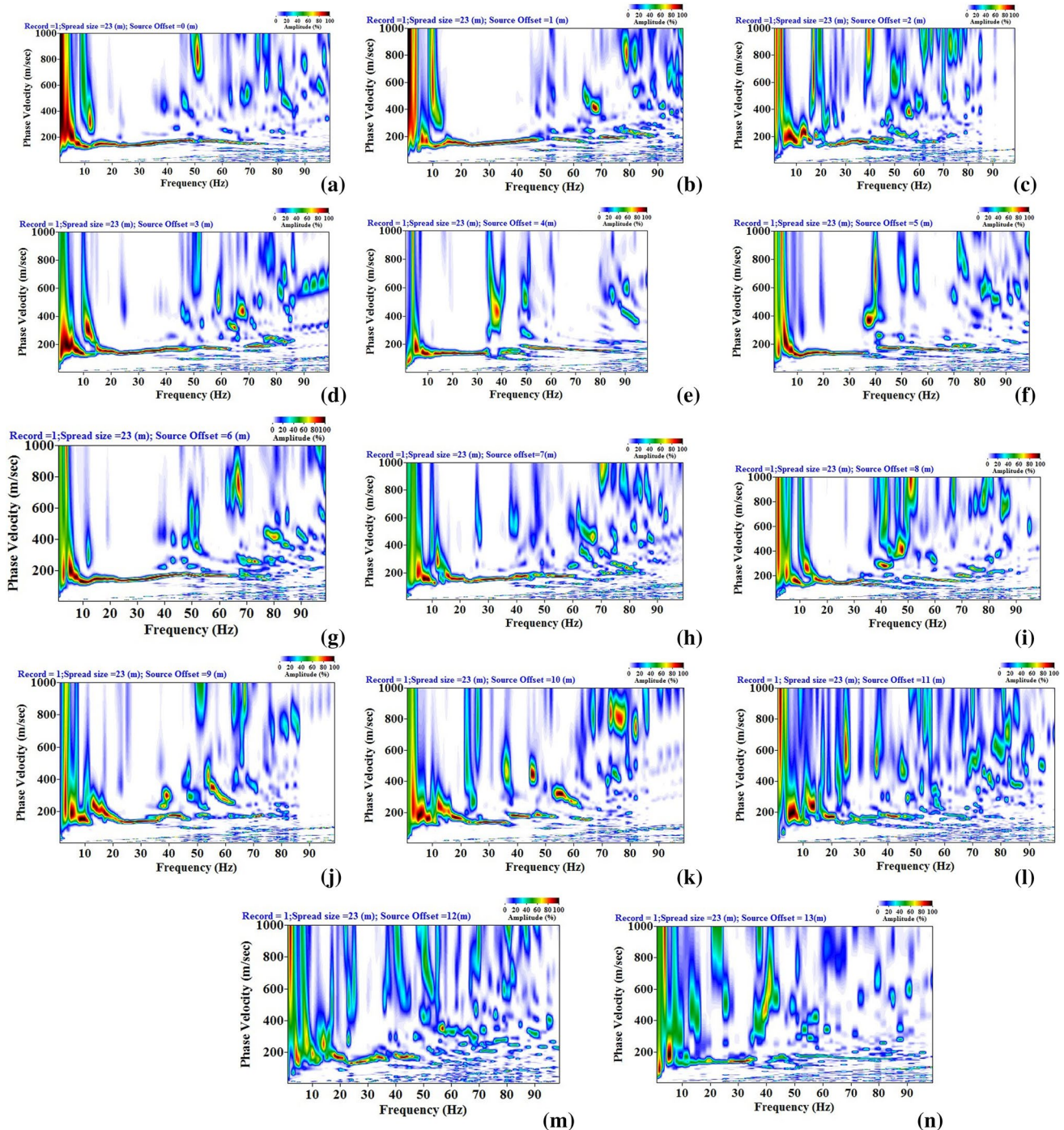


Fig. 19 Dispersion image obtained from active MASW survey conducted with various offset distances **a** 0 m, **b** 1 m, **c** 2 m, **d** 3 m, **e** 4 m, **f** 5 m, **g** 6 m, **h** 7 m, **i** 8 m, **j** 9 m, **k** 10 m, **l** 11 m, **m** 12 m, **n** 13 m

Fig. 20 Comparison of shear wave velocity profiles obtained from borehole survey and that obtained from MASW survey considering various offset distances

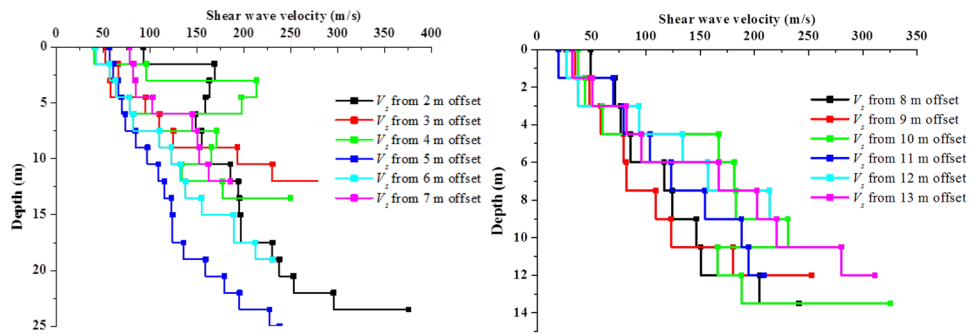
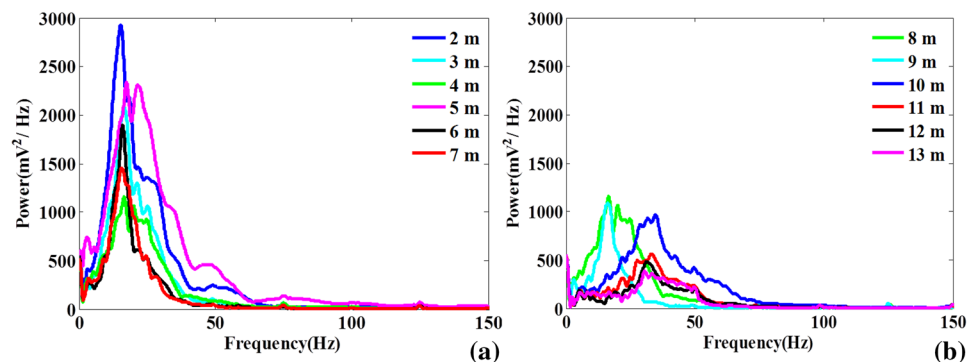


image processing technique adopted on Fig. 19a–d, when inverted, resulted in shear wave velocity profiles exhibited higher deviation from the actual V_s profile obtained from borehole survey (Fig. 1b). The trend of M0 dispersion image becomes distinguishable and continuous for surveys conducted with and offset of 4–6 m (Fig. 19e–g). The corresponding shear Surveys conducted with offsets beyond 6 m exhibited significant noise adulteration which resulted in an indistinguishable and obscure dispersion image. Shear wave velocity profiles obtained with a 5 m offset exhibited the agreeably best match with that obtained from a previously conducted field borehole survey (Fig. 20). The extent of noise adulteration is found to increase with the increase in the offset distance (Fig. 20h–k). Beyond an offset distance of 10 m, the dispersion images failed to provide any useful information from the active MASW survey (Fig. 19l–n). Such adulteration, due to far offset effect, results in low signal-to-noise ratio (SNR) for the extracted dispersion curve, as a result of which shear wave velocity profile is obtained for a significantly curtailed depth of investigation, 5 m for this case. The aim of the present study is to identify a reasonable value of offset distance which provides a good resolution dispersion image with a distinguishable M0 dispersion curve, spread over a wide frequency range, and at the same time, is able to effectively portray the substrata characteristics through the inverted profiles. In this regard, an offset of 5 m proves to be the best choice. However, keeping in mind the practical uncertainties, a choice of 4–6 m offset

can be stated to be sufficient to obtain a good resolution dispersion image for sites comprising heterogeneous materials with less stiffer shallow layers (V_s less than 100 m/s). The averaged power spectrum was also calculated based on the active MASW survey results obtained considering various offset distances to identify the experimental configuration which had produced a sustained energy content spread over a significant frequency band.

Based on Parseval’s theorem and manifestation of averaged power spectrum by Dikmen et al. [11], in the present study, the normalized average power spectra from 13 different linear arrays with varying offset distances were calculated, the inter-receiver spacing being 1 m for each case. The average power spectrum from each test was estimated by averaging the Fourier power spectra of all the 24 traces of each MASW record. Figure 21 represents such a set of averaged power spectrum for an active MASW survey conducted. It is observed that a configuration with 0 and 1 m offsets resulted in power spectrum with incomparably high peak energy as compared to the same obtained with other offsets. Such observation is common due to the significant body wave intrusion in the wavefield owing to the prevalent near-offset effect, and hence, further details of these observations are discarded herein. The PSD obtained from the configurations having offsets of 1–3 m also exhibits high energy, although it quickly degrades for higher frequencies beyond 50 Hz, thus showing the incapability of small offsets to track the effect of higher frequencies in the collected

Fig. 21 Averaged power spectrum estimated from the wavefield records for active MASW survey conducted with various offset distances of a 2, 3, 4, 5, 6 and 7 m b 8, 9, 10, 11, 12 and 13 m



records. Configurations with offsets within the range of 4–10 m recorded significant energy for a very wide frequency band, which inadvertently states that these are the favorable offset ranges that are prone to pick up the Rayleigh wave propagation. Increment of offset beyond 10 m resulted in the incomplete wavefield propagating through the geophone array, owing to the attenuation of energy towards the far end of the array, thus revealing the far-offset effect. Under these conditions, the total energy of the recorded wavefield significantly reduces. Based on the average power spectrum, it can be easily observed that the energy content obtained from an experimental investigation with 5 m offset distance generated signals with sufficiently high energy content spread over a wide band of frequencies (approximately 0–85 Hz). However, considering the practical uncertainties, an offset of 4–6 m can be stated to be best choice as per the site conditions encountered.

Effect of spacing and number of geophones

The inter-receiver spacing has a significant influence on the collected wavefield, and hence affects the resolution of dispersion image. Small geophone spacing controls the high-frequency range of the dispersion image, and is, therefore, related to the resolution at shallow depths. Too close spacing of geophones leads to incomplete wavefield propagation through the geophone array. Hence, it is necessary to increase the receiver spacing for accommodating larger wavelengths in the analysis. However, uncontrolled increase in the receiver spacing or the array length may lead to the development of far-field effects, which may lead to the attenuation of the signals and unwanted adulteration from the prevalent noise wavefields. Hence, it is understood that

there should exist a reasonable receiver spacing, in accordance to the site characteristics, which will lead to achieving the best resolution dispersion image.

Considering various receiver spacings, Fig. 22 exhibits a typical set of wavefields recorded in the field for an experiment conducted with a sampling frequency 15,000 Hz and comprising 5120 samples (i.e., sampling time of 341 ms). It can be observed that, for higher receiver spacing, the waves could not reach most of the geophones at the far side of the array, resulting in significant noise adulteration and rendering a poor and diffused dispersion image. As shown in Fig. 22c, for an inter-receiver spacing 3 m, from the 9th channel onwards, there are practically no active signals, and the traces are substantially contaminated with the prevalent noise. Similar phenomenon can be observed beyond the 13th channel for a spacing of 2 m. Hence, it can be stated that as the inter-receiver spacing increases, larger numbers of geophones fail to participate in providing a proper trace record of the propagating active waves. Figure 22 exhibits a typical condition when the sampling time (341 ms) proves to be just sufficient for recording the complete wave propagation through the geophone array. Similar observations have been made for experiments conducted with sampling frequency 7500 Hz and 5120 samples (i.e., a sampling time 682 ms) where a complete wavefield propagation is noted from the trace records along with severe noise adulteration. The detailed results of the same are not presented herein for the sake of brevity.

Figure 23 shows a set of typical dispersion images developed from the wavefields collected with 5 m offset, and for varying receiver spacings of 1, 2 and 3 m. It is observed that as the receiver spacing increases, there is a significant attenuation of energy leading to loss of information. This

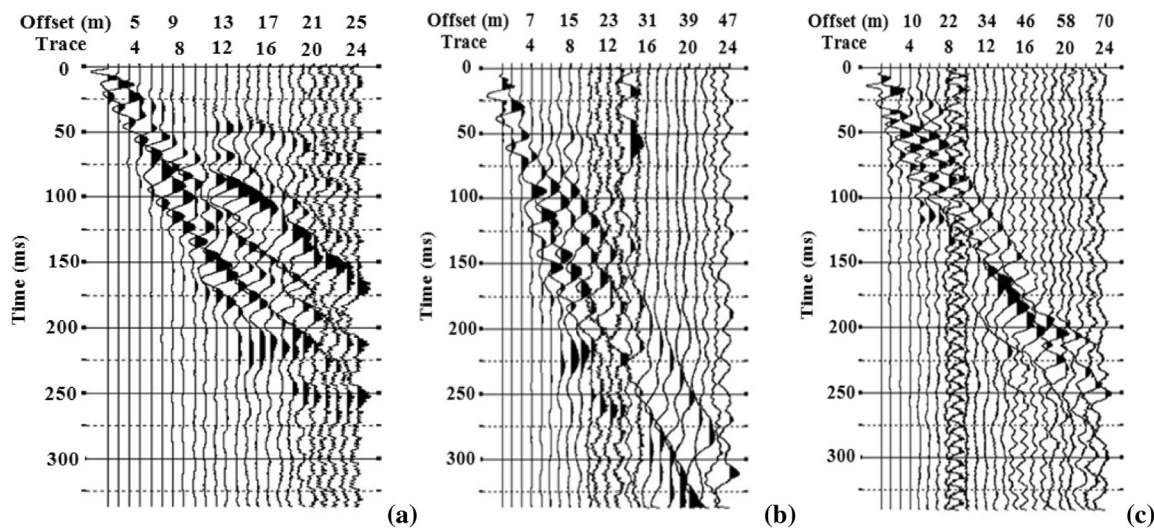


Fig. 22 Traces obtained for survey with 15,000 Hz sampling frequency, 1 m offset distance and receiver spacing of a 1 m, b 2 m and c 3 m

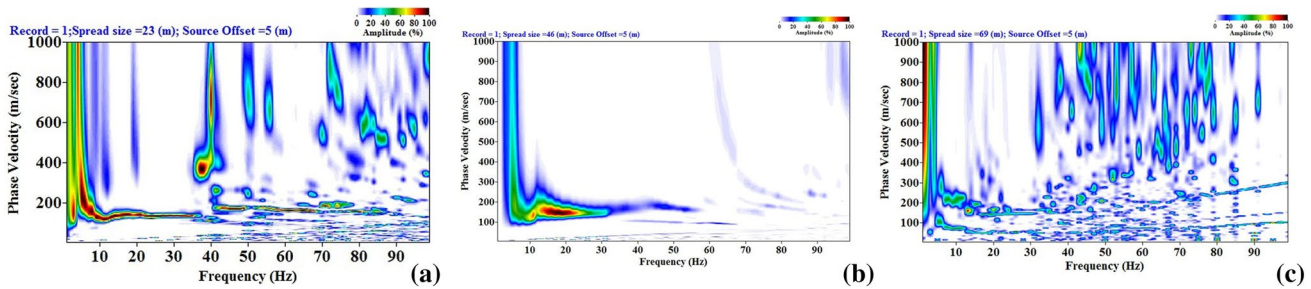


Fig. 23 Typical dispersion images obtained from survey conducted with 5 m offset for a sampling frequency of 15,000 Hz for varying receiver spacing **a** 1 m, **b** 2 m, **c** 3 m

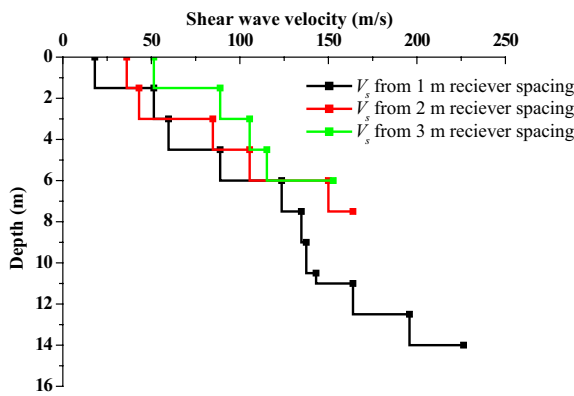


Fig. 24 Shear wave velocity profile obtained from surveys conducted with offset 8 m and varying receiver spacing of 1, 2 and 3 m

is especially noted in the case of dispersion image created with a receiver spacing of 3 m, exhibiting minimal energy spread over the image without portraying any proper dispersion trend. It is aptly clear that a 1 m inter-receiver spacing provided the best resolution image for the study conducted.

Figure 24 shows typical inverted V_s profile obtained from surveys with 1, 2 and 3 m receiver spacing, i.e. a total spread length is 23, 46 and 69 m. In case of 23 and 46 m array length, the depth of investigation is up to 16 and 8 m, respectively. However, with receiver spacing 3 m total depth of investigation is 6 m, which is due to the fact that at 3 m spacing, there is no energy accumulation in the lower frequency range. From the present study, it is observed that the recorded wavelengths (manifested by the depth of investigation) do not merely depend on the maximum spread length. The recorded maximum wavelength is found to be primarily dependent on the frequency characteristics of the substrata medium and the generating source. The dependence of the maximum wavelength on the array length is not as pressing as it is commonly considered. It is a common notion that an increase in the spread length can accommodate larger quantities of the longer wavelengths, thus aiding in attaining the information of the deeper strata. However, it can be stated from the present study that for a given receiver layout, it is

easily possible to perform the analysis considering wavelengths greater than the array length, without violating any sampling theorem.

Another aspect in the field data acquisition is the total number of receiver geophones used in the active MASW survey. It is normally assumed that higher the total number of receiver, the better is the resolution of dispersion images [1, 25]. However, the present study shows that increase of the total number of receivers should be accompanied by increase of array length to get the good resolution dispersion image. Figure 25 shows typical wavefields recorded by 12 and 24 numbers of geophone at a particular site, having an array configuration comprising 5 m offset with 1 m receiver spacing. The corresponding dispersion images are shown in Fig. 26. It can be observed that the dispersion images are nearly similar, although the 24-channel record exhibits more distinctness due to the accumulation of the higher energy in the record. Figure 27 exhibits the dispersion images obtained for a configuration with 2 m receiver spacing. It can be seen that, although obscure (possibly due to noise adulteration), the 24-channel record provides a comparatively better resolution dispersion image than the 12-channel record, and aids in obtaining relatively better information of the substrata. Hence, it can be stated that a higher number of channels can result in a higher resolution dispersion image if, and only if, it is associated with a longer receiver spread. There is no benefit in a mere increase in the number of channels without an increase in the array length.

Effect of source energy

A seismic source generates surface waves (as well as body waves) when it makes an impact on the ground surface. The impact energy is directly related to the range of wavelengths of the generated surface waves, which determines the maximum depth of investigation (Z_{max}). A more powerful source is always needed as a foremost condition for an enhanced investigation depth. A sledgehammer (e.g., ≥ 10 kg) is the most common type of impact source for achieving $Z_{max} \leq 30$ m [10, 11, 13, 15, 16, 19–21, 26,

Fig. 25 Typical wavefields from survey with 2 m offset and 1 m receiver spacing **a** 12 channels, **b** 24 channels

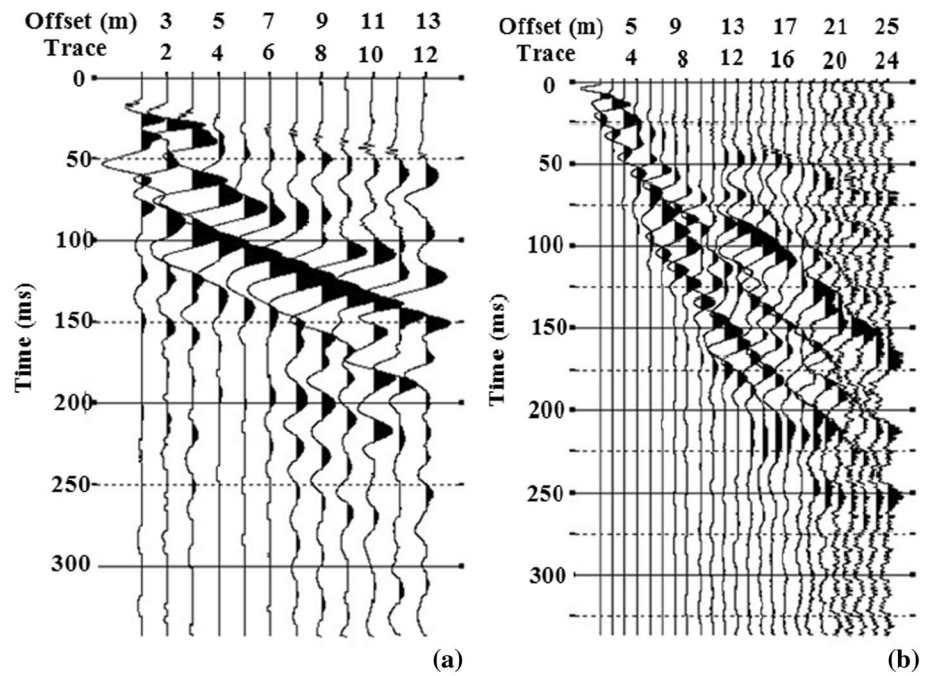


Fig. 26 Dispersion image for active MASW survey with 5 m offset and 1 m receiver spacing using **a** 12 channels, **b** 24 channels

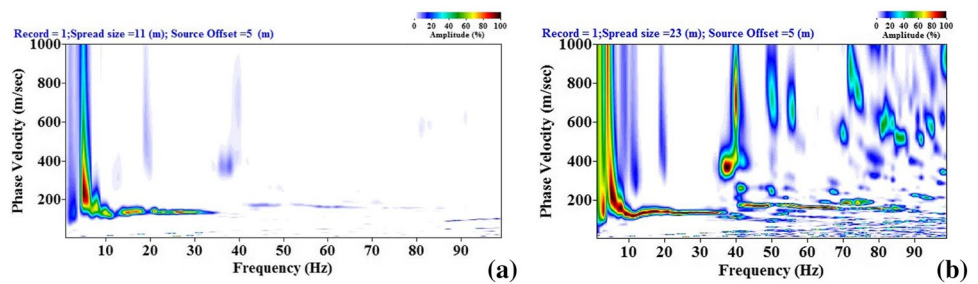
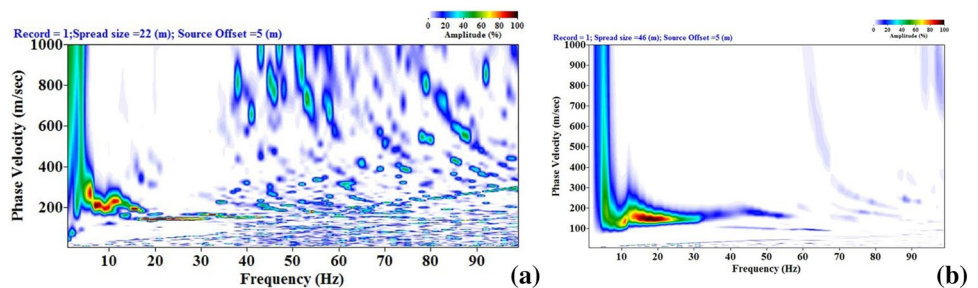


Fig. 27 Dispersion image for active MASW survey with 5 m offset and 2 m receiver spacing using **a** 12 channels, **b** 24 channels



28–31]. An accelerated weight-drop source can increase Z_{max} by 30% under the most favorable conditions [13, 20, 32–34]. A projectile source (e.g., Buffalo Gun) can increase Z_{max} by generating more energy at low frequencies (long wavelengths). Apart from the choice in terms of the Z_{max} , selection of a proper energy source for active MASW survey should also consider other factors such as convenience of use, cost effectiveness, and other regulation issues [5, 21, 24, 27, 30, 35–37]. Energy of different impact sources can be calculated on the basis of their delivered kinetic energy

at the point of impact. If m is the mass of the source (in kg), and v is the velocity of fall of the weight on the ground surface (m/s), the impact energy can be calculated as the Kinetic energy = $0.5 mv^2$ (J). As an example, if the velocity of the fall of hammer is 10 m/s, accordingly, the kinetic energy will be estimated as 250 J for the 10 kg sledgehammer and 2000 J for the 40 kg PEG.

Figure 28 shows the typical power spectra obtained for a single shot of the 10 kg sledgehammer and that of a 40 kg PEG. It can be easily recognized that a single shot with a

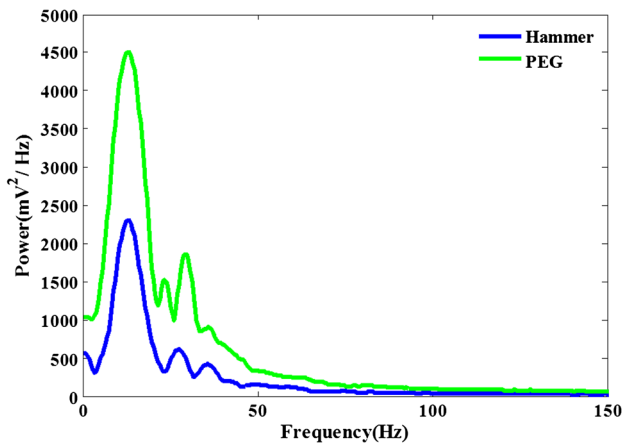


Fig. 28 Typical power spectrum of the signals recorded with 8 kg sledgehammer and 40 kg PEG

40 kg weight dropping PEG has substantially more energy than a sledgehammer. Even at lower frequencies, the presence of high energy renders the heavy-weight PEG to be suitable to provide information of much deeper sub-strata.

The use of an adequate source is primarily governed by the desired depth of investigation. It is worth mentioning that the low frequency content of the signal is necessary to have a larger penetration depth. Figure 29 depicts typical dispersion images obtained from a single strike of a 40 kg PEG and a 10 kg sledgehammer. It can be observed that the dispersion curve generated by the PEG has significant energy content in the low frequency ranges, as compared to the image obtained from the strike of a 10 kg sledgehammer. Along with the higher energy imparted, it had been observed that PEG is able to generate significant low frequency waves (longer wavelengths), thus aiding in larger investigation depths. The weight of the hammer preconditions the frequency content of the generated pulse, and thus, a hammer with lighter weights striking on rigid steel plates produces mostly the high-frequency waves, and hence, provides information only of the relatively shallower depths.

Stacking is a process of combining the dispersion images of various shots so that the resulting dispersion image has higher energy at different frequencies. In this process, even

the energy at the lower frequencies can be substantially increased, so as to obtain shear wave velocity profiles exhibiting higher depths of investigations. Figure 30 exhibits the stacked dispersion images obtained from various numbers of shots the 10 kg sledgehammer. It can be observed that the dispersion image becomes more distinct with the increasing number of stacks, or shot gathers. In general, considering equal velocity and height of fall, the potential energy imparted by a single shot of PEG is nearly 3–4 times higher than a single shot of sledgehammer. In this regard, stacking up the dispersion images from multiple shot gathers of the sledgehammer can be an alternative, yet efficient, approach to generate dispersion images of higher energy. Figure 31 exhibits that the dispersion images obtained from a single shot of PEG and 3-stacked shots of the sledgehammer are very similar in terms of the distribution of the energy along the significant frequencies. Based on the depth of investigation obtained from various stacks, Fig. 32 depicts that the V_s profile obtained from the 3-stacks of the sledgehammer is nearly similar to the same obtained from a single shot of the PEG. It can also be observed that with the increase in the number of stacks, the depth of investigation increases. This observation, thus, establishes that stacking results in an overall increase in the energy content, even at low frequencies, thus rendering larger investigation depths. Hence, from an overall understanding, it can be stated that the energy of the signals recorded at the same site with a single shot of 40 kg PEG can be achieved by 3–4 stacks of the same obtained by the use of a 10 kg sledgehammer. This ensures the applicability of a comparatively lightweight sledgehammer in harnessing the information of deeper substrata using multiple shots and utilizing the strategy of dispersion image stacking.

Conclusions and recommendations

This article elucidates the influences of various data acquisition, pre-processing and processing parameters on the resolution of dispersion image obtained from an active MASW survey. The geophysical investigations have been conducted at a site comprising heterogeneous subsurface and crushed debris. Based on the study, the following conclusions and

Fig. 29 Typical dispersion images obtained from the single strike of a a 40 kg PEG, b 10 kg sledgehammer

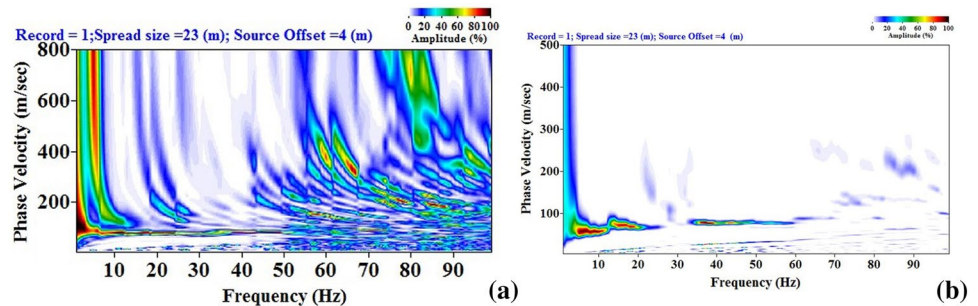


Fig. 30 Typical dispersion images of obtained from stacking of 10 kg sledgehammer records for **a** no stack, **b** single stack, **c** two-stack, **d** three-stack

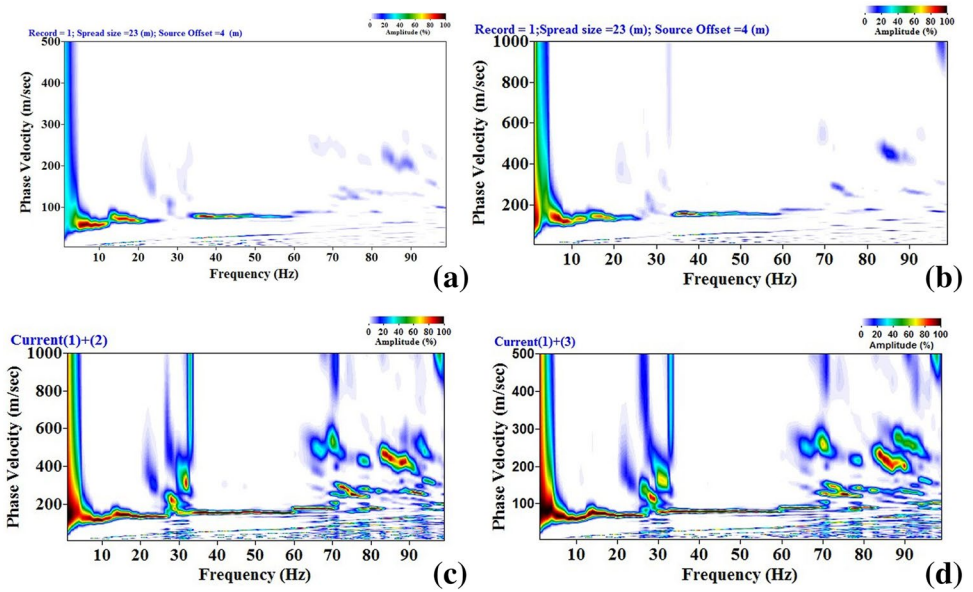


Fig. 31 Comparative of the typical dispersion image obtained from **a** 3-stacked 10 kg sledgehammer record, **b** single shot of 40 kg PEG

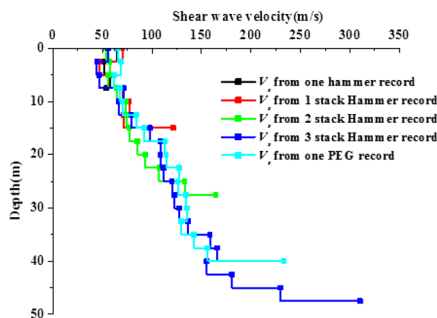
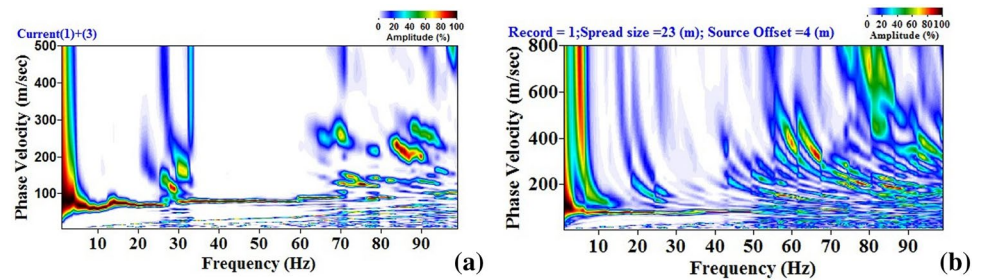


Fig. 32 Comparative of the shear wave velocity profiles obtained from a single shot of 40 kg PEG with different stacks of 10 kg sledgehammer records

recommendations are provided to obtain the best resolution dispersion image from an active MASW survey.

- Optimum sampling time depends on the completion of phase propagation through the receiver array without inducing noise adulteration in the wavefield record. Out of the several combinations of sampling frequency and sampling time, which allow for the optimal completion of

phase propagation, a sample length of 5120 samples and a sampling frequency of 15,000 Hz are recommended.

- Band-pass filter with proper choice of filtering frequency range results in the best resolution of the dispersion image. High-cut filter produces a dispersion image with energy concentrations in truncated lower frequency range. Dispersion images obtained from low-cut and band-stop filters are undecipherable and are not recommended.
- For active MASW survey conducted at any site, combined pre-processing using optimal muting on band-pass filtered wavefield records provides the best resolution wavefield images and results in the dispersion images devoid of aliasing effects.
- The offset distance should be so chosen that the requirement of planar wave propagation is satisfied and the best resolution dispersion image is obtained. Smaller offset distance induces high accumulation of energy at low frequencies resulting in indistinct dispersion trends and shallow depth shear wave velocity profiles (near-offset effect). Large offset distance results in dominant adulteration of the records due to the prevalent noises, resulting in dispersion curves with low SNR (far-offset

effect). The choice of optimal offset distance is site dependent. For sites possessing an average shear wave velocity less than 100 m/s, 4–6 m offset distance is recommended for higher resolution dispersion images. In lieu of the fact that it is difficult to state an absolute optimum offset distance due to the geotechnical and geophysical variations of the site, it is recommended to follow the above offset limits, accompanied by few preliminary trials of active MASW survey in the site.

- Large receiver spacing should be avoided as it leads to significant attenuation of active energy traversing the array, leading to incomplete wave propagation through the array. Even if the entire wave front passes through the array, significant noise signals are recorded in the farthest receivers. This leads to obscure dispersion images with substantially indistinct dispersion trend. Based on the present study, it is recommended to maintain an inter-receiver spacing of 1 m for an active MASW survey to obtain the best resolution dispersion image.
- Inter-receiver spacing and the numbers of receivers used in active MASW survey governs the total length of array. It is found that in contrary to the conventional notion, merely increasing the length of the array will not enhance the depth of investigation. The depth of investigation, governed by the maximum wavelength recorded by the receiver, is primarily dependent on frequency characteristics of the site substrata and the wave generating source. Even if the source generates long wavelengths, the same can get curtailed depending on the site characteristics, and the receivers will be left with shorter wavelength records leading to shallow investigation depths.
- Mere increase in the number of receivers will not enhance the resolution of the dispersion image. An increase in the array length accompanied by an increase in the number of receivers will provide higher resolution dispersion images. Based on the present study, a 24 channel configuration is recommended while satisfying the optimal offset distance and inter-receiver spacing.
- Heavier source such as 40 kg PEG imparts higher impulse energy, nearly 3–4 times that produced by a 10 kg sledgehammer, thus generating wavefields containing longer wavelengths, allowing for higher depths of investigation.
- Since stacking results in the enhancement in the energy of the frequency spectra, dispersion image stacking can be used as an effective means of achieving higher depths of investigation using low weight 10 kg sledgehammers, thus overcoming the difficulty of portability of heavy weight drops for the purpose of active MASW survey. In order to obtain a good resolution dispersion image, it is recommended to use 3–4 dispersion image stacks for sites with $V_{s,30} < 100$ m/s.

References

1. Park CB, Miller RD, Xia J (1998) Imaging dispersion curves of surface waves on multi-channel record. In: Expanded Abstract: Society of Exploration Geophysics, pp 1377–1380
2. Miller RD, Xia J, Park CB, Ivanov J (1999) Multichannel analysis of surface waves to map bedrock. *Lead Edge* 18:1392–1396
3. Xia J, Miller RD, Park CB (1999) Estimation of near-surface shear-wave velocity by inversion of Rayleigh waves. *Geophysics* 64(3):691–700
4. Yilmaz O and Eser M 2002 A unified workflow for engineering seismology. In: 72nd Annual Meeting SEG Salt Lake City UT, pp 1496–1499
5. Tian G, Steeples DW, Xia J, Miller RD, Spikes KT, Ralston MD (2003) Multichannel analysis of surface wave method with the autojuggie. *Soil Dyn Earthq Eng* 23:243–247
6. Tian G, Steeples DW, Xia J, Spikes KT (2003) Useful resorting in surface wave method with the autojuggie. *Geophysics* 68:1906–1908
7. Beaty KS, Schmitt DR, Sacchi M (2002) Simulated annealing inversion of multimode rayleigh wave dispersion curves for geological structure. *Geophys J Int* 151(2):622–631
8. Liu J, Xia J, Luo Y, Li X, Xu S (2004) Extracting transient rayleigh wave and its application in detecting quality of highway roadbed. *Progress in Environmental and Engineering Geophysics*. In: Proceedings of the International Conference on Environmental and Engineering Geophysics (ICEEG)
9. Lin CP, Chang CC, Chang TS (2004) The use of MASW method in the assessment of soil liquefaction potential. *Soil Dyn Earthq Eng* 24:689–698
10. Zhang SX, Chan LS, Xia J (2004) The selection of field acquisition parameters for dispersion images from multichannel surface wave data. *Pure Appl Geophys* 161:185–201
11. Dikmen U, Arisoy M, Akkaya I (2010) Offset and linear spread geometry in the MASW method. *J Geophys Eng* 7:211–222
12. Taipodia J, Baglari D, Dey A (2017) Resolution of dispersion image obtained from active MASW survey. *Disaster Adv* 10(11):34–45
13. Sauvin G, Vanneste M, O'Connor P, O'Rourke S, O'Connell Y, Lombard T, Long M (2016) Impact of data acquisition parameters and processing techniques on S-wave velocity profiles from MASW—Examples from Trondheim, Norway. In: Proceedings of the 17th Nordic Geotechnical Meeting Challenges in Nordic Geotechnic, Reykjavik, pp 1–10
14. Kanli AI, Tildy P, Pronay Z, Pinar A, Hermann L (2006) Vs30 mapping and soil classification for seismic site effect evaluation in Dinar region, SW Turkey. *Geophys J Int* 165:223–235
15. Gosar A, Stopar R, Roser J (2008) Comparative test of active and passive multichannel analysis of surface waves (MASW) methods and microtremor HVSr method. *RMZ Mater Geoenviron* 55(1):41–66
16. Eker AM, Akgun H, Koçkar MK (2012) Local site characterization and seismic zonation study by utilizing active and passive surface wave methods—a case study for the northern side of Ankara, Turkey. *Eng Geol* 151:64–81
17. Dziewonski A, Bloch S, Landisman M (1969) A technique for the analysis of transient seismic signals. *Bull Seismol Soc Am* 59(1):427–444
18. Mitchell BJ (1973) Radiation and attenuation of rayleigh waves from the southeastern Missouri earthquake of October 21 1965. *J Geophys Res* 78:886–899
19. Ivanov J, Park CB, Miller RD, Xia J (2005) Analysing and filtering surface-wave energy by muting shot gathers. *J Environ Eng Geophys* 10:307–322

20. Park CB, Miller RD, Miura H (2002) Optimum field parameters of an MASW survey. In: Expanded Abstract: Japanese Society of Exploration Geophysics, pp 1–6
21. Park CB, Miller RD, Xia J (1999) Multichannel analysis of surface waves. *Geophysics* 64(3):800–808
22. Park CB (2011) Imaging dispersion of MASW data- full vs. selective offset scheme. *J Environ Eng Geophys* 16(1):13–23
23. Stokoe KH II, Wright SG, Bay JA, Roesset JM (1994) Characterization of geotechnical sites by SASW method in geophysical characterization of sites: ISSMFE Technical Committee#10. Oxford Publishers, Oxford, pp 15–25
24. Xu Y, Xia J, Miller RD (2006) Quantitative estimation of minimum offset for multichannel surface-wave survey with actively exciting source. *J Appl Geophys* 59:117–125
25. Moro DG, Pipan M, Forte E, Finetti I (2003) Determination of Rayleigh wave dispersion curves for near surface applications in unconsolidated sediments. In: Expanded Abstracts: Society of Exploration Geophysicists, pp 1247–1250
26. Shtivelman V (2003) Using surface waves for studying the shallow subsurface. *Bollettino di Geofisica Teorica ed Applicata* 44:223–236
27. Park CB, Miller RD, Xia J (2001) Offset and resolution of dispersion curve in multichannel analysis of surface waves. In: Proceedings of SAGEEP SSM1-SSM, 4: 1–6
28. Xia J, Xu Y, Miller RD (2007) Generating an image of dispersive energy by frequency decomposition and slant stacking. *Pure Appl Geophys* 164:941–956
29. Park CB, Miller RD, Xia J, Ivanov J (2007) Multichannel analysis of surface waves (MASW)—active and passive methods. *Lead Edge* 26:60–64
30. Wood CM, Cox BR (2012) A comparison of MASW dispersion uncertainty and bias for impact and harmonic sources. In: Geotronics, ASCE, pp 2756–2765
31. Srinivas GS, Goverdhan K, Narsimhulu CH, Seshunarayana T (2014) Estimation of shear wave velocity in drifts using multichannel analysis of surface wave (MASW) technique—a case study from Jammu & Kashmir, India. *J Geol Soc India* 84:174–180
32. Stephenson WJ, Louie JN, Pullammanappallil S, Williams RA, Odum JK (2005) Blind Shear-wave velocity comparison of ReMi and MASW results with boreholes to 200 m in Santa Clara Valley: implications for earthquake ground-motion assessment. *Bull Seismol Soc Am* 95(6):2506–2516
33. Park CB, Miller RD, Xia J, Ivanov J (2002) Seismic characterization of geotechnical sites by Multichannel Analysis of Surfaces Waves (MASW) method. In: KGS Experiences in Seismic Surveying, pp 1–16
34. Park CB, Miller RD, Ryden N, Xia J, Ivanov J (2005) Combined use of active and passive surface waves. *J Environ Eng Geophys* 10(5):323–334
35. Xia J, Miller RD, Park CB, Ivanov J (2000) Construction of 2-D vertical shear-wave velocity field by the multichannel analysis of surface wave technique. In: Proceedings of the Symposium on the application of geophysics to engineering and environmental problems, pp 1197–1206
36. Kaufmann RD, Xia J, Benson RC, Yuhr LB, Casto DW, Park CB (2005) Evaluation of MASW data acquired with a hydrophone streamer in a shallow marine environment. *J Environ Eng Geophys* 10:87–98
37. Neducza B (2007) Stacking of surface waves. *Geophysics* 72(2):51–58